Analysis Note: Study of $\psi' \rightarrow \pi^+\pi^- J/\psi$

F. A. Harris
Department of Physics and Astronomy
The University of Hawaii
2505 Correa Road
Honolulu, HI 96822
USA

Sept. 2, 1998

Introduction

The process $\psi' \rightarrow \pi^+\pi^- J/\psi$ can be investigated using the very clean, high statistics $\psi' \rightarrow \pi^+\pi^- J/\psi$, $J/\psi \rightarrow l^+l^-$ events. For this case, the dipion invariant mass distribution is very different from that expected from phase space [1], and a number of authors have proposed various theoretical models [2]-[6]. The reaction may be pictured as the radiation of two gluons by the quarkonium system as it transfers to the lower energy level, followed by the hadronization of the gluons into pions.

There is increased interest in this process because of the problems with the $\Upsilon(3S) \rightarrow \pi^+\pi^-\Upsilon(1S)$ [7], which has a peak at low mass, as well as a peak at high mass. This distribution looks very different than $\psi' \rightarrow \pi^+\pi^- J/\psi$, which has a high mass peak, and most theoretical models. The process $\Upsilon(2S) \rightarrow \pi^+\pi^-\Upsilon(1S)$ is similar to $\psi' \rightarrow \pi^+\pi^- J/\psi$ but not the same.

In this paper, we will use the $\psi' \rightarrow \pi^+\pi^- J/\psi$ process to test models. This is the third in a series of informal analysis notes, and much of the background necessary for this paper is described in more detail in the first two notes [8] [9] and in Ref. [10].

Cuts

Pion Cuts:

The initial pion cuts are the same as in Ref. [8] but are given again for convenience. We require a pair of oppositely charged candidate pion tracks that satisfy:

1. good run (PPRUNS: status > 1)

2. mnfit = 2, -9, -19

3. $|\cos\theta_\pi| < 0.75$. Here θ_π is the polar angle of the π in the laboratory system.

4. $p_\pi < 0.5$ GeV/c, where p_π is the pion momentum.

5. $pxy_\pi > 0.1$ GeV/c, where pxy_π is the momentum of the pion transverse to the beam direction. This removes tracks that circle in the Main Drift Chamber.

6. $\cos\theta_{\pi\pi} < 0.9$, where $\theta_{\pi\pi}$ is the laboratory angle between the π^+ and π^-. This cut is used to eliminate contamination from misidentified e^+e^- pairs from γ conversions.

7. $3.0 < m_{recoil} < 3.2$ GeV/c^2. m_{recoil} is the mass recoiling against the $\pi\pi$ system.

These are the cuts used to select events for determining $B(J/\psi \to l^+l^-)$, where a fit is done to extract the number of $\psi^{'} \to \pi^+\pi^- J/\psi$, $J/\psi \to l^+l^-$ and $J/\psi \to$ anything events. However, when selecting a sample for other purposes, like studying $\psi^{'} \to \pi^+\pi^- J/\psi$, additional cuts are made on the π's to reduce background. The additional cuts are:

1. $\Sigma Hit_\pi^{dE/dx} > 13$. $\Sigma Hit_\pi^{dE/dx}$ is the number of hits used in the dE/dx calculation.

2. $|\chi_\pi^{dE/dx}| < 3.0$. $\chi_\pi^{dE/dx} = \frac{(dE/dx)_{meas} - (dE/dx)_{exp}}{\sigma}$ where $(dE/dx)_{meas}$ and $(dE/dx)_{exp}$ are the measured and expected dE/dx energy losses for pions, respectively, and σ is the experimental dE/dx resolution.

Lepton Cuts

We require four tracks total with the sum of the charge equal zero. The lepton tracks must satisfy:

1. $0.5 < p_l < 2.5$ GeV/c. Here p_l is the three-momenta of the candidate lepton track.

2. $|\cos\theta_e| < 0.75$, $|\cos\theta_\mu| < 0.60$. Here θ_e and θ_μ are the laboratory polar angles of the electron and muon, respectively. This cut ensures that electrons are contained in the BSC and muons in the MUID system.

3. $\cos\theta_{l^+l^-} < -0.85$. This is the cosine of the angle between the two leptons in the lab. The leptons from this decay are almost back to back.

4. $\cos\theta_{l^+l^-}^{cm} < -0.975$. This is the cosine of the angle between the two leptons in the J/ψ CM. The leptons are even more back-to-back in the CM system.

5. p_{l^+} or $p_{l^-} > 1.3$ GeV/c or $p_{l^+} + p_{l^-} > 2.4$ GeV/c. This cut selects events consistent with J/ψ decay, while rejecting background.

6. For e^+e^- candidate pairs: SCE_+ and $SCE_- > 0.6$ GeV/c, where SCE is the energy deposited in the BSC, or, if one of the tracks goes through a BSC rib or has $P_l < 0.8$ GeV/c, the dE/dx information of both tracks in the MDC must be consistent with that expected for electrons. The rib region of the BSC is not used because the Monte Carlo does not model the energy deposition well in this region.

7. For $\mu^+\mu^-$ pair candidates at least one track must have $N^{hit} > 1$, where N^{hit} is the number of MUID layers with matched hits and ranges from 0 to 3. If only one track is identified in this fashion, then the invariant mass of the $\mu\mu$ pair must also be within 250 MeV/c^2 of the J/ψ mass.

Additional Cuts

We make additional cuts in order to reduce background from events where the low energy pions undergo $\pi \to \mu\nu$ decay or where the leptons (especially electrons) radiate much of their energy. These cuts are necessary for comparisons with theoretical models.

1. good tracks: mfit = 2
2. vertex cuts:
   (a) $|rm(\pi)| < 0.015m$
   (b) $|zm(\pi)| < 0.15m$
   (c) $|zm(\pi^+) - zm(\pi^-)| < 0.05m$
3. $3.07 < m_{recoil} < 3.12$ GeV/c^2
4. $|m_{l^+l^-} - m_{J/\psi}| < 0.25$ GeV/c^2

A total of about 22.8 K events remains after these cuts, compared to 32.7 K fitted events found in the $B(J/\psi \to l^+l^-)$ paper[10]. Fig. 1a shows the m_{recoil} distribution using only the initial cuts, and Fig. 1b shows this distribution using all cuts except the additional m_{recoil} cut (additional cut 3). The background remaining after these cuts is estimated to be less than 0.3 %.

Monte Carlo

The Monte Carlo generator used is PPGEN. A total of 200,000 (153 realization) plus 370,000 (154 realization) Monte Carlo events are generated each for the $\psi' \to \pi^+\pi^- J/\psi$, $J/\psi \to e^+e^-$ and $\psi' \to \pi^+\pi^- J/\psi$, $J/\psi \to \mu^+\mu^-$ samples. The Monte Carlo[11] assumes:

1. Sequential 2-body decays: $\psi' \to X + J/\psi$, $X \to \pi^+\pi^-$, and $J/\psi \to l^+l^-$.
2. The mass of the $\pi\pi$ system is weighted towards high mass.
$$\frac{d\sigma}{dm_{\pi\pi}} \propto (\text{phase space}) \times (m_{\pi\pi}^2 - 4m_\pi^2)^2$$
3. The orbital angular momentum between the $\pi\pi$ system and the J/ψ and between the π's in the $\pi^+\pi^-$ system is 0.
4. X and J/ψ are uniformly distributed in $\cos\theta$ in the incoming e^+e^- rest frame, which is the same as the laboratory frame.

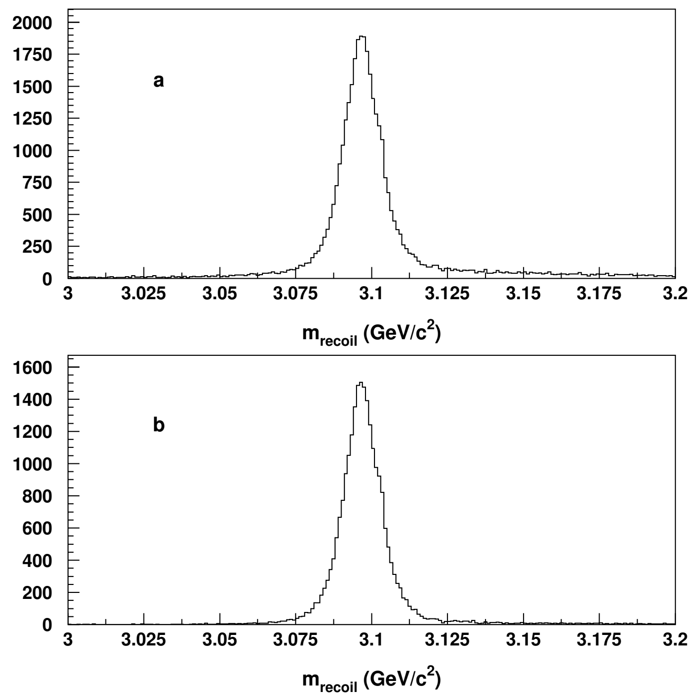

Figure 1: **a)** Number of events versus $m^{recoil}_{\pi^+\pi^-}$, the mass recoiling against the two π's, for $\psi(2S) \to \pi^+\pi^- J/\psi$, $J/\psi \to l^+l^-$ events where only the initial cuts (see text) are used. **b)** Number of events versus $m^{recoil}_{\pi^+\pi^-}$ where all cuts are used except for the final m_{recoil} cut.

5. π's are uniformly distributed in $\cos\theta^*_\pi$, where θ^*_π is the angle between the J/ψ direction and the π^+ in the X rest frame.

6. Leptons have $1+\cos^2\theta^*_l$ distribution, where θ^*_l is the angle between the beam direction and the positive lepton in the J/ψ rest frame.

7. J/ψ decay has order α^3 final state radiative correction in the rest frame of the J/ψ.

Comparison with Monte Carlo Distributions

In Ref. [9], comparisons were made between data and Monte Carlo data for various distributions. In general the agreement was good, indicating that the cuts eliminated most background and that the Monte Carlo did a reasonable job of representing the data. However some distributions, like the $m_{\mu^+\mu^-}$ distribution, did not agree well, possibly indicating an inadequacy in the realization.

Here we compare other distributions to check whether the assumptions made by the Monte Carlo are correct. In order to be able to compare to theoretical models, we correct the distributions for detection efficiency. Monte Carlo data is run through the same analysis program as the data. A bin-by-bin efficiency is then determined for each distribution of interest using the generated and detected Monte Carlo data. This bin-by-bin efficiency is then used to correct each bin of the data distributions [12].

In Fig. 2, we see reasonable agreement between data and Monte Carlo except in Fig. 2d, which is the distribution of the cosine of the angle between the π^+ and the J/ψ direction in the rest frame of the $\pi\pi$ system, $\cos\theta^*_{\pi^+}$. The flat Monte Carlo distribution is due to the assumption that the relative angular momentum of the 2 π's is S-wave. The disagreement between data and Monte Carlo data casts doubt on this assumption.

Fig. 2a indicates that the $m_{\pi\pi}$ distribution agrees fairly well but not perfectly with the assumed empirical distribution [13]. Fig. 2b indicates agreement with the assumed $1+\cos^2\theta^*_l$ distribution for the leptons in $\psi' \to \pi^+\pi^- J/\psi$, $J/\psi \to l^+l^-$ events. The flat distribution in Fig. 2c is related to the assumption that the relative angular momentum between the $\pi\pi$ system and the J/ψ is zero.

Fig. 3 shows the ϕ angle distributions for the l^+ in the lab, the J/ψ in the lab, and the π^+ in the rest frame of the $\pi\pi$ system.

$$\phi^*_{\pi^+} = \arctan[\frac{(\widehat{(\widehat{\hat{X} \times \hat{z}}) \times \hat{X}}) \cdot \hat{p_{\pi^+}}}{(\widehat{\hat{X} \times \hat{z}}) \cdot \hat{p_{\pi^+}}}]$$

All distributions are uniform in ϕ, consistent with the Monte Carlo assumptions.

Since Fig. 2d indicates an inadequacy with the Monte Carlo, it is necessary to correct our bin-by-bin efficiency determination in our following studies. We will use the Novikov-Shifman model (discussed below), which gives a reasonable approximation to the data, to determine a weighting for Monte Carlo events so that the proper efficiency is determined as a function of $\cos\theta^*_\pi$ and $m_{\pi\pi}$.

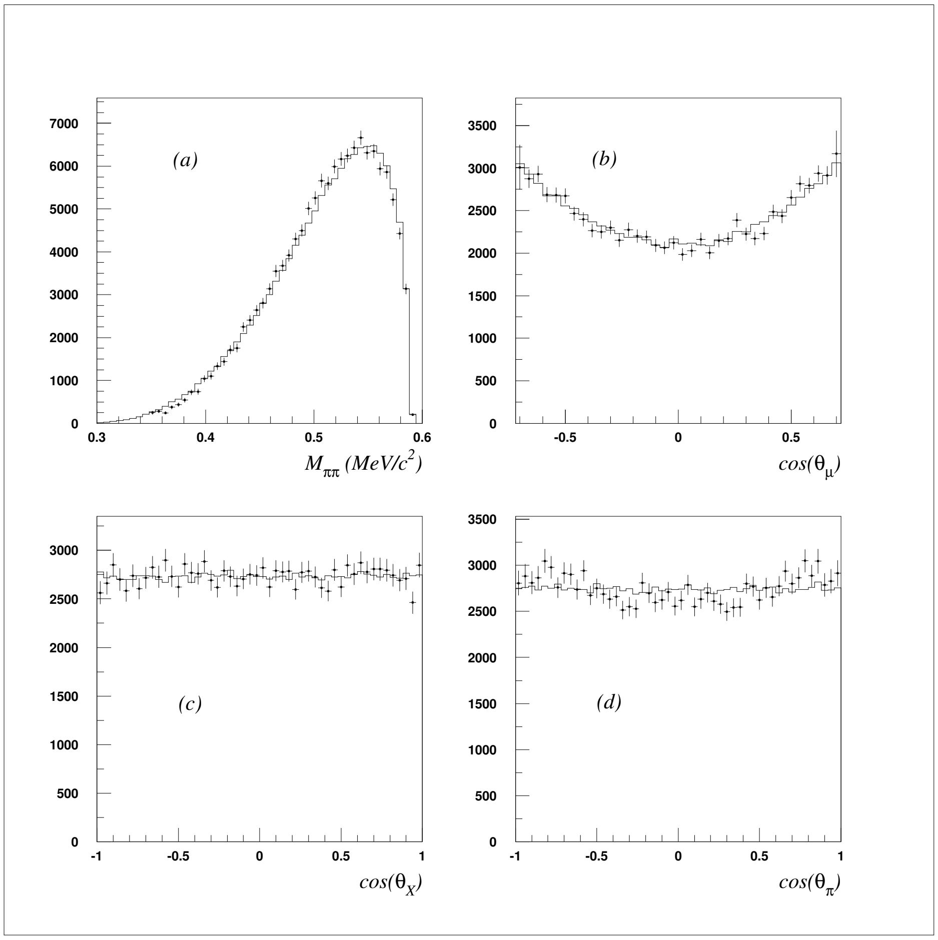

Figure 2: Various distributions (corrected for detection efficiency) for $\psi' \to \pi^+\pi^- J/\psi$, $J/\psi \to l^+l^-$ decays. **a.)** $m_{\pi^+\pi^-}$ distribution. The distribution is in fair but not perfect agreement with the assumed empirical distribution. **b.)** $\cos\theta_l^*$ distribution. The assumed distribution is a $1+\cos^2\theta_l^*$ distribution. This angle is the angle between the beam direction and the e^+ in the rest frame of the J/ψ. **c.)** $\cos\theta_X$ distribution. This is the cosine of the angle of the $\pi\pi$ system with respect to the e^+e^- direction in the incoming e^+e^- CM system. The distribution for Monte Carlo data is flat because of the S-wave assumption for the relative angular momentum of the $\pi\pi$ system and the J/ψ. **d.)** $\cos\theta^*_{\pi^+}$ distribution. This is the cosine of the angle of the π^+ with respect to the J/ψ direction in the $\pi\pi$ rest frame. The Monte Carlo distribution is flat because of the assumption that the relative angular momentum of the π's is S-wave. The data agree well with the Monte Carlo except in d.).

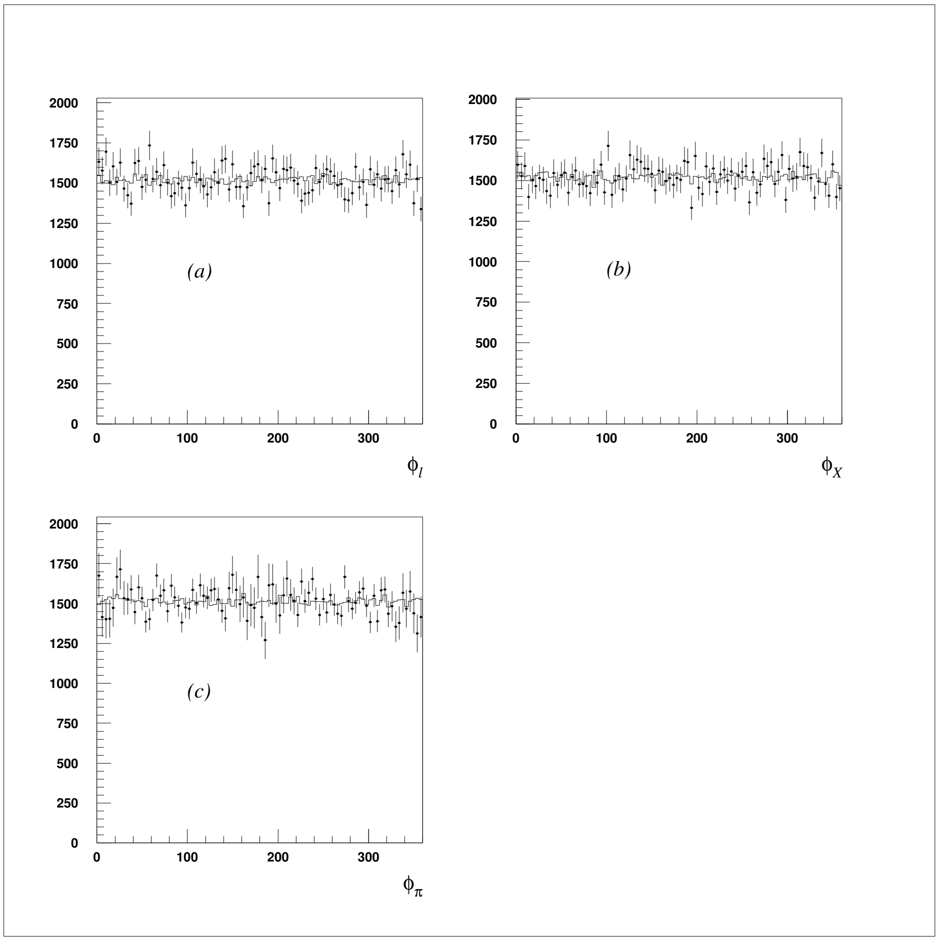

Figure 3: Azimuthal angle distributions (corrected for detection efficiency) for $\psi' \to \pi^+\pi^- J/\psi$, $J/\psi \to l^+l^-$ decays. a.) The ϕ angle distribution for the l^+ in the lab. b.) The ϕ angle distribution for the J/ψ in the lab. c.) The ϕ angle distribution for the π^+ in the $\pi\pi$ rest frame.

Angular Distributions in $\psi' \to \pi^+\pi^- J/\psi$

Partial Wave Analysis

In this section, we will compare our angular distributions with the general decay amplitude analysis of Cahn [14]. The ψ' and ψ have $J^P = 1^-$ and $I^{GC} = 0^{--}$, while the $\pi\pi$ system has $I^{GC} = 0^{++}$. At an e^+e^- machine, the ψ' is produced with polarization transverse to the beam. The decay of ψ' is treated as a 2-body decay:

$$\psi' \to XJ/\psi, X \to \pi^+\pi^-,$$

which can be described by the quantum numbers:

$\vec{\boldsymbol{l}}$ – $\pi\pi$ angular momentum

$\vec{\boldsymbol{L}}$ – ψ X angular momentum

$\vec{\boldsymbol{s}}$ – spin of ψ

$\vec{\boldsymbol{s}}\,'$ – spin of the ψ'

Defining $\vec{S} = \vec{s} + \vec{l}$, called the channel spin, then $\vec{s}\,' = \vec{S} + \vec{L} = \vec{s} + \vec{l} + \vec{L}$. An eigenstate of $J^2 = s'^2$, L^2, S^2, and J_z may be constructed. Parity conservation and charge conjugation invariance require both L and l to be even.

The decay can be described in terms of partial waves. Cahn works out the angular distributions in terms of partial wave amplitudes, $M_{l,L,S}$. The partial waves can be truncated after a few terms. He says, "For the purpose of demonstration, and with simplicity as a criterion, consider only M_{001}, M_{201}, and M_{021}". Cahn's 1-dimensional distributions:

$$\frac{d\Gamma}{d\Omega_\psi} \propto [|M_{001}|^2 + |M_{201}|^2 + \frac{1}{4}|M_{021}|^2(5 - 3\cos^2\theta^*_\psi)] \tag{1}$$

$$\frac{d\Gamma}{d\Omega_\pi} \propto [|M_{001}|^2 + \frac{1}{4}|M_{201}|^2(5 - 3\cos^2\theta^*_\pi) + |M_{021}|^2] \tag{2}$$

$$\frac{d\Gamma}{d\Omega_\mu} \propto [|M_{001}|^2(1 + \cos^2\theta^*_\mu) + \frac{1}{10}(|M_{201}|^2 + |M_{021}|^2)(13 + \cos^2\theta^*_\mu)] \tag{3}$$

The $d\Omega$'s are measured in their respective rest frames. It is understood that the $M_{l,L,S}$ are functions of $m_{\pi\pi}$.

It turns out that Eqns. 1 and 2 are incorrect! This is suggested by Fig. 2d. We see that the data indicates that the distribution is concave upwards, while Eqn. 2 would suggest that the distribution must be concave downwards if M_{201} is nonzero. It is nice to have data to check theory!

To find the correct 1D distributions, we start with Cahn's full expression [14], which we assume is correct. We then integrate over $d\Omega_\mu$ using Mathematica and find:

$$\frac{d\Gamma}{d\Omega_\pi d\Omega_\psi} \propto |M_{001}|^2 + |M_{201}|^2(\frac{5}{4} - \frac{3}{4}\cos^2\theta^*_\pi) + |M_{021}|^2(\frac{5}{4} - \frac{3}{4}\cos^2\theta^*_\psi)$$

$$
\begin{aligned}
&+2\Re\{M_{201}M^*_{001}\}[\frac{1}{\sqrt{2}}(\frac{3}{2}\cos^2\theta^*_\pi - \frac{1}{2})] \\
&+2\Re\{M_{021}M^*_{001}\}[\frac{1}{\sqrt{2}}(\frac{3}{2}\cos^2\theta^*_\psi - \frac{1}{2})] \\
&+2\Re\{M_{201}M^*_{021}\}[\frac{9}{8}\sin^2\theta^*_\pi \sin^2\theta^*_\psi \cos 2(\phi^*_\pi - \phi^*_\psi) \\
&+\frac{9}{16}\sin 2\theta^*_\pi \sin 2\theta^*_\psi \cos(\phi^*_\pi - \phi^*_\psi) \\
&+\frac{1}{2}(\frac{3}{2}\cos^2\theta^*_\pi - \frac{1}{2})(\frac{3}{2}\cos^2\theta^*_\psi - \frac{1}{2})]
\end{aligned} \tag{4}
$$

This agrees with Cahn except for obvious typos. We can then integrate to get the corrected 1-D distributions:

$$
\frac{d\Gamma}{d\Omega_\psi} \propto [|M_{001}|^2 + |M_{201}|^2 + \frac{1}{4}|M_{021}|^2(5 - 3\cos^2\theta^*_\psi) + \frac{1}{\sqrt{2}}\Re\{M_{021}M^*_{001}\}(3\cos^2\theta^*_\psi - 1)] \tag{5}
$$

$$
\frac{d\Gamma}{d\Omega_\pi} \propto [|M_{001}|^2 + \frac{1}{4}|M_{201}|^2(5 - 3\cos^2\theta^*_\pi) + |M_{021}|^2 + \frac{1}{\sqrt{2}}\Re\{M_{201}M^*_{001}\}(3\cos^2\theta^*_\pi - 1)] \tag{6}
$$

Two of Cahn's 1D distributions (Eqns. 1 and 2) dropped the interference term. It is the interference term in Eqn. 6 that allows the equation to be consistent with the data. Eqn. 3 is correct.

Fits to 1D Angular Distributions

There are too many unknowns to fit the 1D distributions separately, but we can fit them simultaneously. There are 3 complex numbers to be obtained. According to Cahn, if the ψ' and ψ are regarded as inert, then the usual final state argument gives $M_{l,L,S} = e^{i\delta^0_l(m_{\pi\pi})}|M_{l,L,S}|$, where $\delta^0_l(m_{\pi\pi})$ is the isoscalar phase shift for quantum number l. If we interpolate the S wave, isoscalar phase shift data found in [15], we find $\delta^0_0 \approx 45^o$. Actually δ^0_0 is a function of $m_{\pi\pi}$. Also δ^0_2 is supposed to be ≈ 0. Using these values as input, we obtain the combined fit shown in Fig. 4 and the results given in Table 1. The fitting procedure also uses two parameters (not shown), which correspond to the relative normalizations of the second and third distributions relative to the first. Also given in Table 1 are the ratios $|M_{201}|/|M_{001}|$ and $|M_{021}|/|M_{001}|$.

We have also tried to obtain δ^0_0, as well as the three real amplitudes. Cahn points out that one of the advantages of the process $\psi' \to \pi^+\pi^- J/\psi$ is that it allows us to obtain δ^0_0, which is not well measured in this mass range. The results from the fit are given in Table 2. Minuit indicates that there are problems with the fit. However, both fits yield a nonzero result for $|M_{201}|$, indicating non negligible D-wave in the $\pi\pi$ system. The amplitude $|M_{021}|$ is very small, indicating the the ψX angular momentum is consistent with zero.

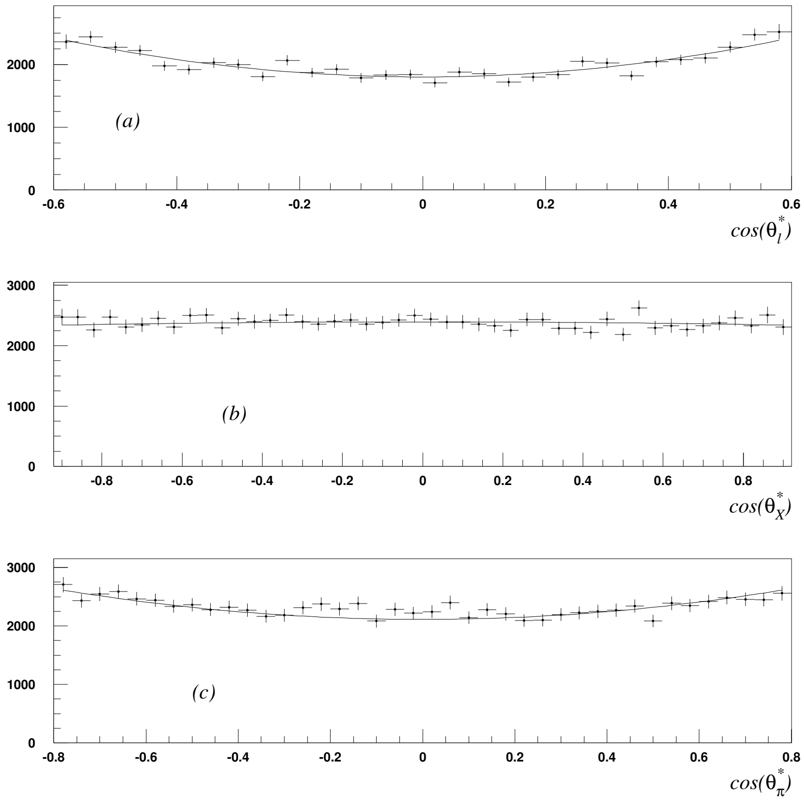

Figure 4: Simultaneous fits (χ^2) to three 1-D histograms of a.) $\cos\theta^*_\mu$, b.) $\cos\theta^*_X$, and c.) $\cos\theta^*_\pi$ using Eqns. 3, 5, and 6, respectively. The phase shifts used are $\delta^0_0 = 45^o$ and $\delta^0_2 = 0^o$.

Table 1: Results of simultaneous χ^2 fits to the three 1-D distributions of $\cos\theta^*_\mu$, $\cos\theta^*_X$, and $\cos\theta^*_\pi$ shown in Fig. 4. The phase shifts used are $\delta^0_0 = 45^o$ and $\delta^0_2 = 0^o$. The amplitude normalizations are arbitrary. Two other fit parameters (not shown) are the normalizations of the second and third distributions relative to the first.

$\|M_{001}\|$	$41.6 \pm 0.4 \pm 0.8$
$\|M_{201}\|$	$7.5 \pm 1.4 \pm 1.2$
$\|M_{021}\|$	$-0.56 \pm 0.60 \pm 0.48$
$\|M_{201}\|/\|M_{001}\|$	$0.18 \pm 0.03 \pm 0.03$
$\|M_{021}\|/\|M_{001}\|$	$-0.014 \pm 0.014 \pm 0.012$
χ^2/DF	0.8

Table 2: Results of simultaneous χ^2 fits to the three 1-D distributions of $\cos\theta^*_\mu$, $\cos\theta^*_X$, and $\cos\theta^*_\pi$ using Eqns. 3, 5, and 6. Here an attempt is made to determine the phase shift δ^0_0 from the fit. The phase shift δ^0_2 is taken to be 0^o. The amplitude normalizations are arbitrary. Two other fit parameters (not shown) are the relative normalizations of the second and third distributions relative to the first. Note that Minuit indicates that the fit has problems. The errors shown are statistical only.

$\lvert M_{001}\rvert$	42.0 ± 0.4
$\lvert M_{201}\rvert$	5.0 ± 2.5
$\lvert M_{021}\rvert$	-0.55 ± 0.61
δ^0_0	0 ± 56^o
$\lvert M_{201}\rvert/\lvert M_{001}\rvert$	0.12 ± 0.06
$\lvert M_{021}\rvert/\lvert M_{001}\rvert$	-0.013 ± 0.014
χ^2/DF	0.8
Fit result:	problems

Fits to the 2D Distribution

We can integrate Eqn. 4 over the ϕ angles to obtain an expression that depends only on $\cos\theta^*_\pi$ and $\cos\theta^*_\psi$:

$$\begin{aligned}\frac{d\Gamma}{d\cos\theta^*_\pi d\cos\theta^*_\psi} \propto\ & |M_{001}|^2 + |M_{201}|^2(\frac{5}{4} - \frac{3}{4}\cos^2\theta^*_\pi) + |M_{021}|^2(\frac{5}{4} - \frac{3}{4}\cos^2\theta^*_\psi) \\ & +2\Re\{M_{201}M^*_{001}\}[\frac{1}{\sqrt{2}}(\frac{3}{2}\cos^2\theta^*_\pi - \frac{1}{2})] \\ & +2\Re\{M_{021}M^*_{001}\}[\frac{1}{\sqrt{2}}(\frac{3}{2}\cos^2\theta^*_\psi - \frac{1}{2})] \\ & +\Re\{M_{201}M^*_{021}\}[(\frac{3}{2}\cos^2\theta^*_\pi - \frac{1}{2})(\frac{3}{2}\cos^2\theta^*_\psi - \frac{1}{2})] \qquad (7)\end{aligned}$$

We can then fit the 2D distribution of $\cos\theta^*_\pi$ versus $\cos\theta^*_\psi$ using this equation. We first fit assuming $\delta^0_0 = 45^o$ and $\delta^0_2 = 0^o$, as was done previously. Using these values, we obtain the fit values shown in Table 3. The 1D projections of the 2D distribution along with the fit projections are shown in Fig. 5.

We have also performed the fits for different $m_{\pi\pi}$ intervals for $\delta^0_2 = 0^o$ and values of δ^0_0 that depend on the $m_{\pi\pi}$ interval[16]. The results are shown in Table 4, along with the value of δ^0_0 used. The ratios $|M_{201}|/|M_{001}|$ and $|M_{021}|/|M_{001}|$ do not show large variations between the three intervals, and $|M_{201}|/|M_{001}|$ is inconsistent with zero for all intervals.

Table 3: Result of the 2-D Likelihood fit to $\cos\theta^*_\pi$ versus $\cos\theta^*_X$ using Eqn. 7. The phase shifts used are $\delta^0_0 = 45^o$ and $\delta^0_2 = 0^o$. The amplitude normalizations are arbitrary.

$\|M_{001}\|$	$13.6 \pm 0.08 \pm 0.25$
$\|M_{201}\|$	$2.3 \pm 0.5 \pm 0.5$
$\|M_{021}\|$	$0.05 \pm 0.22 \pm .19$
$\|M_{201}\|/\|M_{001}\|$	$0.17 \pm 0.04 \pm 0.04$
$\|M_{021}\|/\|M_{001}\|$	$0.004 \pm 0.02 \pm 0.01$
χ^2/DF	1.1

We can also assume that δ^0_2 is zero and fit for δ^0_0. The results of this fit is shown in Table 5. Note that PAW says that this fit has problems, so the results are not meaningful.

In comparing the results from Tables 1-5, we see that $|M_{201}|/|M_{001}|$ varies between 0.12 and 0.18 and is at least two sigma from zero. On the other hand $|M_{021}|/|M_{001}|$ varies between 0 and 0.06 and is, in almost all cases, consistent with zero. Only for the lowest $m_{\pi\pi}$ region is it more than one standard deviation from zero. When we try to fit for δ^0_0, the fits have problems in Minuit. We are unable to determine the phase angle.

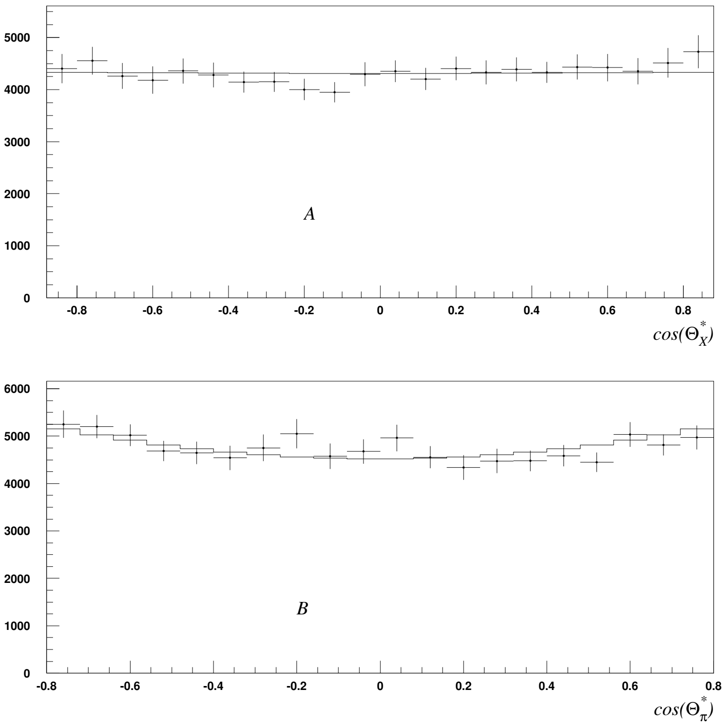

Figure 5: Likelihood fit result for $\cos\theta_X^*$ versus $\cos\theta_\pi^*$ using Eqn. 7. The phase shifts used are $\delta_0^0 = 45^o$ and $\delta_2^0 = 0^o$. a.) The projection of $\cos\theta_X^*$ and the fit result. b.) The projection of $\cos\theta_\pi^*$ and the fit result. Points with error bars are the data; the histogram is the fit result.

Table 4: Results of the 2-D Likelihood fits to $\cos\theta_\pi^*$ versus $\cos\theta_X^*$ using Eqn. 7 for different $m_{\pi\pi}$ intervals. The amplitude normalization is arbitrary. Here the value of δ_0^0 used depends on the $m_{\pi\pi}$ interval. $\delta_2^0 = 0$.

$m_{\pi\pi}$ Range (GeV/c^2)	0.36 - 0.5	0.5 - 0.54	0.54 - 0.6
δ_0^0 used as input	27^o	42^o	51^o
$\lvert M_{001}\rvert$	$8.36 \pm 0.06 \pm 0.27$	$7.43 \pm 0.06 \pm 0.11$	$7.86 \pm 0.10 \pm 0.13$
$\lvert M_{201}\rvert$	$1.19 \pm 0.37 \pm 0.90$	$0.89 \pm 0.41 \pm 0.22$	$1.37 \pm 0.50 \pm 0.24$
$\lvert M_{021}\rvert$	$0.53 \pm 0.27 \pm 0.40$	$-0.27 \pm 0.21 \pm 0.12$	$0.14 \pm 0.20 \pm 0.21$
$\lvert M_{201}\rvert/\lvert M_{001}\rvert$	$0.14 \pm 0.04 \pm 0.11$	$0.12 \pm 0.06 \pm 0.03$	$0.17 \pm 0.06 \pm 0.03$
$\lvert M_{021}\rvert/\lvert M_{001}\rvert$	$0.06 \pm 0.03 \pm 0.05$	$-0.04 \pm 0.03 \pm 0.02$	$0.02 \pm 0.03 \pm 0.03$
χ^2/DF	1.3	1.5	1.3
Events	6186	7075	9362

Table 5: Result of the 2-D Likelihood fit to $\cos\theta^*_\pi$ versus $\cos\theta^*_X$ using Eqn. 7. Here an attempt is made to determine the phase shift δ^0_0 from the fit. The amplitude normalization is arbitrary. The errors here are statistical only.

$\lvert M_{001}\rvert$	13.68 ± 0.14
$\lvert M_{201}\rvert$	1.85 ± 0.7
$\lvert M_{021}\rvert$	0.05 ± 0.22
$\lvert M_{201}\rvert/\lvert M_{001}\rvert$	0.14 ± 0.05
$\lvert M_{021}\rvert/\lvert M_{001}\rvert$	0.0 ± 0.02
δ^0_0	32 ± 33^o
χ^2/DF	1.1
Fit result	problems

Simple Model Independent Fit of the $\cos\theta^*_\pi$ Distribution as a Function of $m_{\pi\pi}$

The amount of D wave as a function of $m_{\pi\pi}$ has been fit using

$$N(\cos\theta) \propto 1.0 + p * (\cos^2\theta - 1/3) + q * (\cos^2\theta - 1/3)^2 \tag{8}$$

The last term corresponds to the amount of D-wave, while the middle term corresponds to the interference term[17]. The results are shown in Fig. 6 and in Table 6. It can be seen that q is very small and is consistent with zero. The behavior of the interference term, p, as a function of $m_{\pi\pi}$ is shown in Fig. 7. Also shown in this figure is the prediction of the Novikov-Shifman model, which is described later.

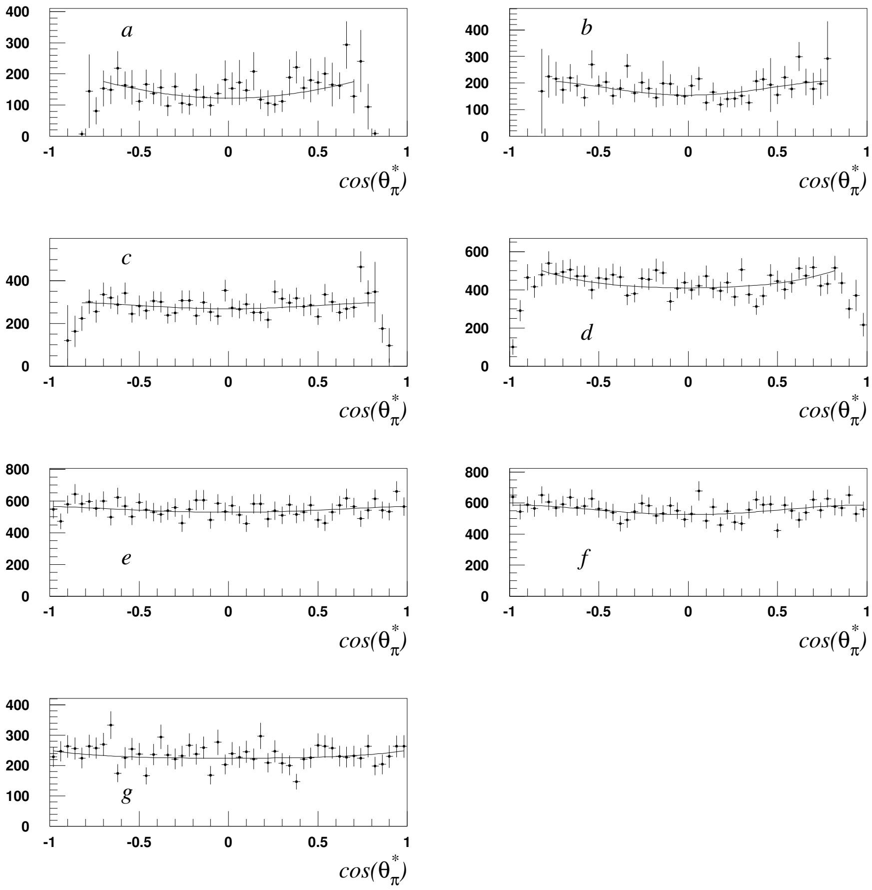

Figure 6: Fits of $\cos\theta^*_\pi$ using Eqn. 8 as a function of $m_{\pi\pi}$. The fit results are shown in Table 6. **a)** $0.34 < m_{\pi\pi} < 0.42$ GeV/c^2, **b)** $0.42 < m_{\pi\pi} < 0.45$ GeV/c^2, **c)** $0.45 < m_{\pi\pi} < 0.48$ GeV/c^2, **d)** $0.48 < m_{\pi\pi} < 0.51$ GeV/c^2, **e)** $0.51 < m_{\pi\pi} < 0.54$ GeV/c^2, **f)** $0.54 < m_{\pi\pi} < 0.57$ GeV/c^2, and **g)** $0.57 < m_{\pi\pi} < 0.60$ GeV/c^2,

Table 6: Fit results to $\cos\theta^*_\pi$ distribution using a χ^2 fit to Eqn. 8. The fit also requires a normalization term which is not shown.

$m_{\pi\pi}$ Range (GeV/c^2)	p	q	χ^2/DOF	Events
0.34 - 0.42	$0.67 \pm 0.67 \pm 0.75$	$-0.1 \pm 2.4 \pm 2.4$	0.7	894
0.42 - 0.45	$0.41 \pm 0.38 \pm 0.59$	$-0.6 \pm 1.5 \pm 1.7$	0.8	1122
0.45 - 0.48	$0.15 \pm 0.16 \pm 0.08$	$-0.16 \pm 0.74 \pm 0.78$	0.8	1995
0.48 - 0.51	$0.30 \pm 0.10 \pm 0.05$	$0.18 \pm 0.51 \pm 0.23$	0.8	3729
0.51 - 0.54	$0.08 \pm 0.06 \pm 0.03$	$-0.04 \pm 0.19 \pm 0.05$	0.7	5620
0.54 - 0.57	$0.15 \pm 0.05 \pm 0.04$	$-0.13 \pm 0.17 \pm 0.08$	1.0	6403
0.57 - 0.60	$0.08 \pm 0.09 \pm 0.05$	$0.07 \pm 0.28 \pm 0.18$	1.0	2959

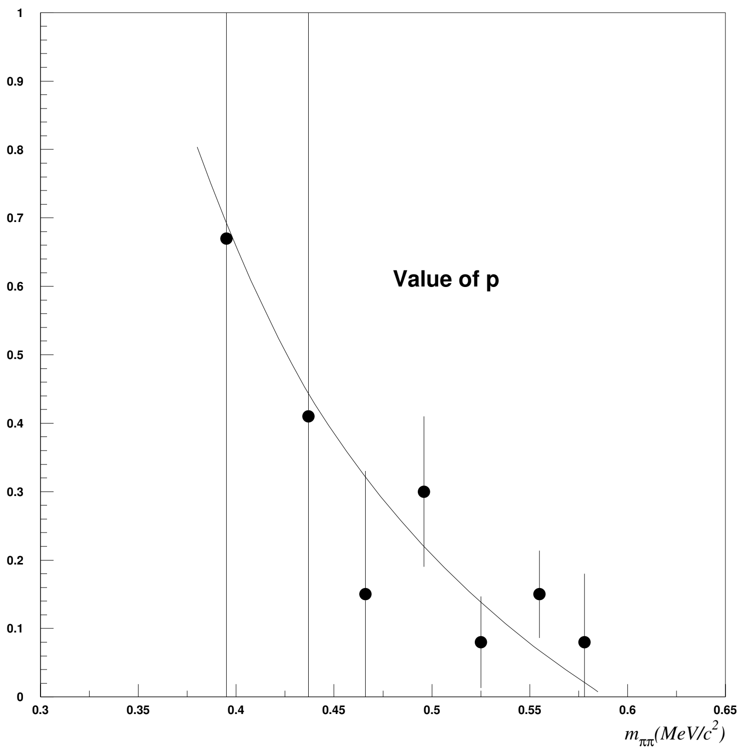

Figure 7: Plot of the interference term, p, from Eqn. 8 versus $m_{\pi\pi}$. The smooth curve is the prediction of the Novikov-Shifman model (described later).

ARGUS-type Fit of the $\cos\theta^*_\pi$ Distribution

ARGUS [19] and CLEO [20] have fit the $\cos\theta^*_\pi$ distribution for $\Upsilon(2S) \rightarrow \pi^+\pi^-\Upsilon(1S)$ to a coherent sum of J = 0 and J =2, J$_z$ = 0 waves [19]:

$$\frac{dN}{d\cos\theta^*} = N|\sqrt{1-|\varepsilon|^2}Y_0^0 + \varepsilon Y_2^0|^2$$

ARGUS obtains a solution with Re $\varepsilon = 0.018 \pm 0.009$ and the Im ε is 0 with a large error. If the phase is free, they get $|\varepsilon| = 0.018^{+0.018}_{-0.009}$. If $\pi\pi$ rescattering is negligible, ε is expected to be real. CLEO finds $\varepsilon = 0.042 \pm 0.022$.

If we fit this equation for the $\psi(2S)$ case, we obtain:

$$|\varepsilon| = 0.026^{+0.076}_{-0.007}$$

$$\theta = 0 \pm 74^o,$$

where Re $\varepsilon = |\varepsilon| \cos\theta$, etc. We also find that the best fit corresponds to the imaginary part being 0 with a large error.

Comparison with Heavy Quarkonium Models

Novikov-Shifman Model

The first comparison of BES data with Heavy Quark models was presented at BES95 by Fan Jingyun [18]. The model investigated was the Novikov-Shifman [3] model, which has the amplitude:

$$\begin{aligned} A &\propto \{q^2 - \kappa(\Delta M)^2(1 + \frac{2m_\pi^2}{q^2}) \\ &\quad + \frac{3}{2}\kappa[(\Delta M)^2 - q^2](1 - \frac{4m_\pi^2}{q^2})(\cos^2\theta_\pi^* - \frac{1}{3})\}, \end{aligned} \tag{9}$$

where q is the 4 momentum of the dipion system and $\Delta M = M_{\psi'} - M_{J/\psi}$. The parameter κ is given by:

$$\kappa = (b/6\pi)\alpha_s(\mu)\rho_\mu^G(\mu), \tag{10}$$

where $b = 9$ is the first expansion coefficient of the Gell-Mann-Low function, ρ^G is the gluon share of the π's momentum, which is about 0.4, and κ is predicted to be ≈ 0.15 to 0.2 [4]. From Eqn. 10, it can be seen that κ is expected to be different for $\psi(2S)$ decays and the decays of other charmonia, because of the running of α_s. The first terms in the amplitude are the S-wave contribution, and the last term is the D-wave contribution. Note that parity and charge conjugation invariance require that the spin be even. If κ is non-zero, it is predicted that there should be some D-wave. However, since κ is expected to be small, the process should be predominantly S-wave.

The differential cross section is obtained by squaring the amplitude and multiplying by phase space.

$$\frac{d\Gamma}{dm_{\pi\pi}d\cos\theta_\pi^*} \propto (\mathrm{PS}) \times A^2. \tag{11}$$

where

$$PS = \sqrt{\frac{(m_{\pi\pi}^2 - 4m_\pi^2)[M_{J/\psi}^4 + M_{\psi'}^4 + m_{\pi\pi}^4 - 2(M_{J/\psi}^2 m_{\pi\pi}^2 + M_{\psi'}^2 m_{\pi\pi}^2 + M_{J/\psi}^2 M_{\psi'}^2)]}{4M_{\psi'}^2}}$$

By integrating over one variable at a time, it is possible to obtain the following 1D equations for the $m_{\pi\pi}$ invariant mass spectrum and the $\cos\theta^*_\pi$ distribution:

$$\begin{aligned}\frac{d\sigma}{dm_{\pi\pi}} &\propto |\vec{q}|\sqrt{(q^2-4m_\pi^2)}\{[q^2-\kappa(\Delta M)^2(1+\frac{2m_\pi^2}{q^2})]^2 \\ &\quad +0.2\kappa^2[(\Delta M)^2-q^2]^2(1-\frac{4m_\pi^2}{q^2})^2\} \qquad (12)\\ \frac{d\sigma}{d\cos\theta^*_\pi} &\propto \{1.322-4.8597\kappa+5.1577\kappa^2+1.18296\kappa(\cos^2\theta^*_\pi-\frac{1}{3}) \\ &\quad -2.65421\kappa^2(\cos^2\theta^*_\pi-\frac{1}{3})+0.3738\kappa^2(\cos^2\theta^*_\pi-\frac{1}{3})^2\} \qquad (13)\end{aligned}$$

The $m_{\pi\pi}$ distribution is fit using Eqn. 12, as shown in Fig. 8a. The fit yields $\kappa = 0.186 \pm 0.003$ with a $\chi^2/\mathrm{DOF} = 1.2$. We have fit the $\cos\theta$ distribution in the region $-0.8 < \cos\theta^*_\pi < 0.8$ using Eqn. 13. The results are shown in Fig. 8b. The fit yields $\kappa = 0.23^{+0.07}_{-0.04}$ with a $\chi^2/\mathrm{DOF} = 0.7$.

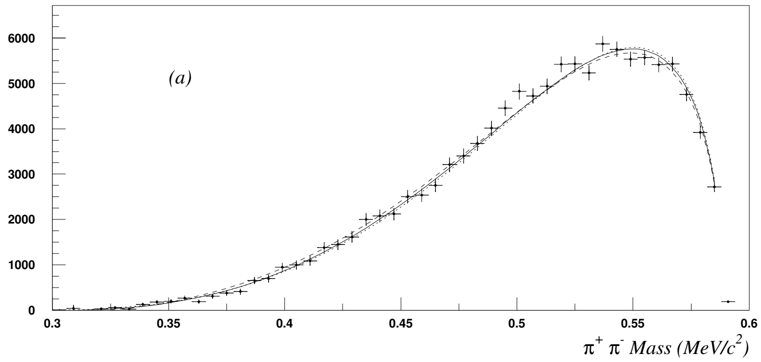

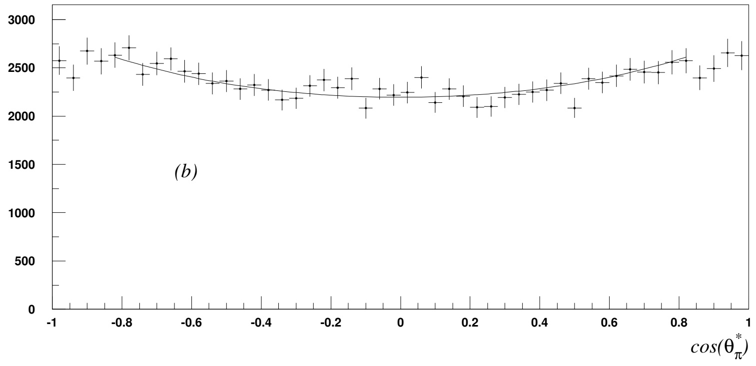

Figure 8: Fits to distributions. The results are given in Tables 7 and 8. **(a)** $m_{\pi\pi}$ distribution. The points are the data corrected for efficiency, and the curves are the fit results. The smooth curve is the Novikov-Shifman model (Eqn. 12). The long-dashed curve is the T. M. Yan model without higher order corrections (Eqn. 14), and the short-dashed curve is the Voloshin-Zakarov model (Eqn. 15). **(b)** $\cos\theta^*_\pi$ distribution. The points are the data corrected for efficiency, and the curve is the fit result (Eqn. 13).

Table 7: Fit results for κ for the Novikov-Shifman model.

Distribution	κ	χ^2/DOF
$m_{\pi\pi}$ (Fig. 8a)	$0.186 \pm 0.003 \pm 0.010$	1.2
$\cos\theta_\pi^*$ (Fig. 8b)	$0.23^{+0.07}_{-0.04} \pm 0.09$	0.7
$m_{\pi\pi}$ vs $\cos\theta_\pi^*$ (Fig. 9)	$0.183 \pm 0.003 \pm 0.005$	1.2

We have also fit the joint $\cos\theta_\pi^*$ and $m_{\pi\pi}$ distribution (Eqn. 11), as shown in Fig. 9. This method is preferable to the previous 1D fits because any $\cos\theta_\pi^*$ - $m_{\pi\pi}$ correlation is used in the fit. Using this approach, we obtain a $\kappa = 0.183 \pm 0.003$ and a $\chi^2/DOF = 1.2$. The results of the different fits are in good agreement. and are summarized in Table 7.

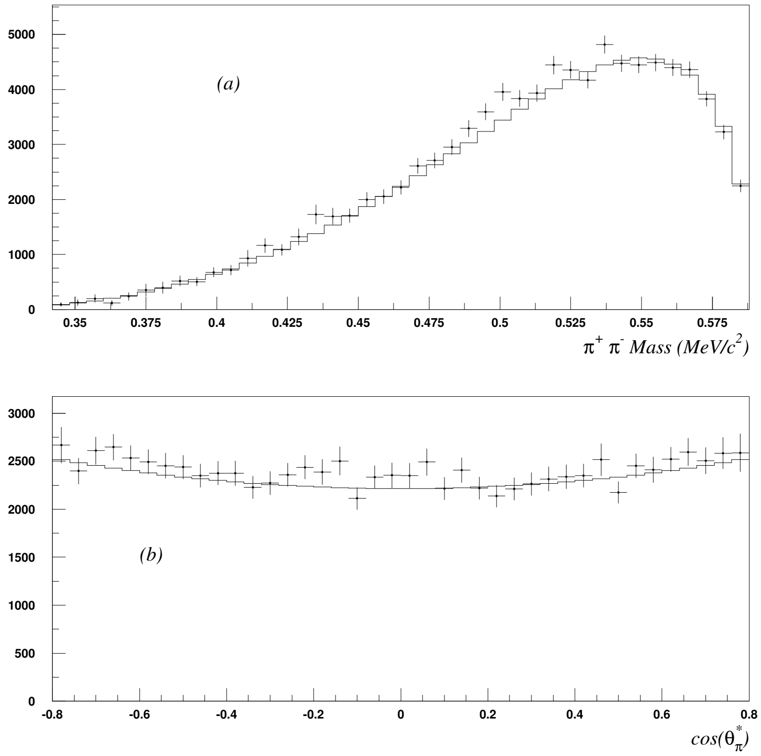

Figure 9: Fit of the 2D $\cos\theta_\pi^*$ versus $m_{\pi\pi}$ distribution to Eqn 11. **(a)** The 2D distribution projected in $m_{\pi\pi}$. **(b)** The 2D distribution projected in $\cos\theta_\pi^*$. The points are the data corrected for efficiency, and the curve is the projected fit result.

Using Eqns. 9 and 11, where we write in Eqn. 9 $A = A_S + A_D$, the ratio of the D-wave transition rate to the total rate can be obtained

$$R_D = \frac{\int dq^2 \int_{-1}^{1} d\cos\theta(PS)|A_D|^2}{\int dq^2 \int_{-1}^{1} d\cos\theta(PS)|A_S + A_D|^2}$$

The limits of the q^2 integration are $q^2_{min} = 4m_\pi^2$ and $q^2_{max} = (M_{\psi'} - M_{J/\psi})^2$. For the value of

κ obtained from the 2D fit, we obtain

$$R_d = 0.184\%$$

T. M. Yan and Voloshin-Zakorov Models

Other models which describe the $m_{\pi\pi}$ invariant mass spectrum are the T. M. Yan Model [5]:

$$\begin{aligned} \frac{d\sigma}{dm_{\pi\pi}} &\propto (PS) \times [(m_{\pi\pi}^2 - 2m_\pi^2)^2 + \frac{B}{3A}(m_{\pi\pi}^2 - 2m_\pi^2)(m_{\pi\pi}^2 - 4m_\pi^2 \\ &\quad +2K^2(1 + \frac{2m_\pi^2}{m_{\pi\pi}^2})) + O(\frac{B^2}{A^2})], \end{aligned} \tag{14}$$

where

$$K = \frac{M_{\psi'}^2 - M_{J/\psi}^2 + m_{\pi\pi}^2}{2M_{\psi'}}$$

and the Voloshin - Zakarov Model [2]

$$\frac{d\sigma}{dm_{\pi\pi}} \propto (PS) \times [m_{\pi\pi}^2 - \lambda m_\pi^2]^2. \tag{15}$$

In the T. M. Yan model, the term $O(\frac{B^2}{A^2})$ refers to higher order (HO) terms.

The $m_{\pi\pi}$ invariant mass spectrum has been fit with these models, as shown in Fig. 8a. As can be seen, the Novikov-Shifman and the Voloshin-Zakorov models give nearly identical fits. The T. M. Yan model, neglecting higher order terms does not agree as well with the data. Including the higher order terms [5], however, gives a fit result which is nearly identical to the other two models, as seen in Fig. 10. All the results are summarized in Table 8, along with the $\psi(2S)$ results from Argus [19], which used $\psi(2S)$ data from Mark II. Argus did not fit the T. M. Yan model with the HO corrections, but we agree well on the results of the fits that they did do.

T. Mannel - M. L. Yan Model

Mannel has constructed an effective Lagrangian using chiral symmetry arguments to describe the decay of heavy excited S-wave spin-1 quarkonium into a lower S-wave spin-1 state [21]. Using total rates, as well as the invariant mass spectrum from Mark II via ARGUS [19], the parameters of this theory have been obtained. More recently, M. L. Yan *et al.* have pointed out that this model allows D-wave [22], like the Novikov-Shifman model. In this model, the amplitude can be written

$$\begin{aligned} A &\propto \{q^2 - c_1(q^2 + |\vec{q}|^2)(1 + \frac{2m_\pi^2}{q^2}) + c_2 m_\pi^2\} \\ &\quad + \frac{3}{2}[c_1|\vec{q}|^2(1 - \frac{4m_\pi^2}{q^2})](\cos^2\theta_\pi^* - \frac{1}{3}), \end{aligned} \tag{16}$$

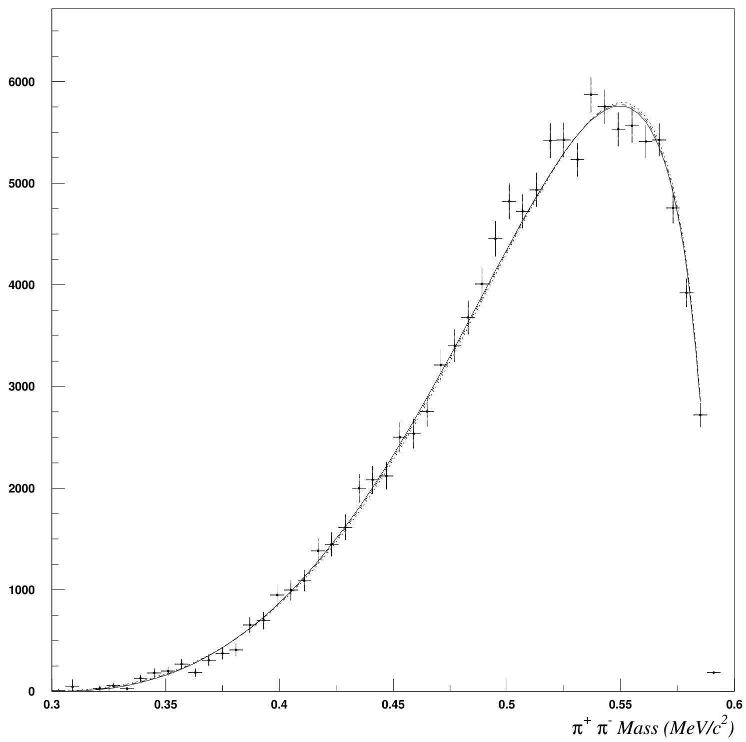

Figure 10: Fits to the $m_{\pi\pi}$ distribution. The points are the data corrected for efficiency, and the curves are the fit results. The smooth curve is the Novikov-Shifman model (Eqn. 12). The long-dashed curve is the T. M. Yan model with higher order corrections [5], and the short-dashed curve is the Voloshin-Zakarov model (Eqn. 15). The three models are nearly indistinguishable. The results are summarized in Table 8.

Table 8: Fit Results for the $m_{\pi\pi}$ distribution.

Model	BES	Argus - MKII [19]
Novikov-Shifman	$\kappa = 0.186 \pm 0.003 \pm 0.010$ $\chi^2/DOF = 1.2$	0.194 ± 0.010 38/24
T. M. Yan	$B/A = -0.225 \pm 0.004 \pm 0.015$ $\chi^2/DOF = 1.9$	-0.21 ± 0.01
T. M. Yan (HO)	$B/A = -0.336 \pm 0.009 \pm 0.022$ $\chi^2/DOF = 1.3$	
Voloshin	$\lambda = 4.35 \pm 0.06 \pm 0.22$ $\chi^2/DOF = 1.5$	

where

$$c_1 = -\frac{g_1}{3g}(1 + \frac{g_1}{6g})^{-1}$$

$$c_2 = 2(\frac{g_3}{g} - \frac{g_1}{3g} - 1)(1 + \frac{g_1}{6g})^{-1} \quad (17)$$

The first term in Eqn. 16 is the S-wave term, and the second is the D-wave term. Note that another constant in the effective Lagrangian, g_2, has been taken to be zero since it is suppressed by the chiral symmetry breaking scale. This amplitude is very similar to Eqn. 9 but contains an extra term proportional to m_π^2.

We have fit the joint $\cos\theta_\pi^*$ - $m_{\pi\pi}$ distribution using the amplitude of Eqn. 16, as shown in Fig. 11. We obtain:

$$\frac{g_1}{g} = -0.517^{+0.076}_{-0.100} \pm 0.159$$
$$\frac{g_3}{g} = 0.644^{+0.374}_{-0.285} \pm 0.26$$

with a $\chi^2/DOF = 1.18$.

In the chiral limit, $g_3 = 0$. If we fit with this value for g_3, we obtain

$$\frac{g_1}{g} = -0.347 \pm 0.007$$

with a $\chi^2/DOF = 1.18$. Here the error is the statistical error only. The results for both cases are given in Table 9, along with the results from Ref.[21].

Table 9: Fit results using Eqn 16. In the second fit, g_3 is set to zero.

	g_1/g	g_3/g	χ^2/DOF
This Exp.	$-0.517^{+0.076}_{-0.100} \pm 0.159$	$0.644^{+0.374}_{-0.285} \pm 0.26$	1.18
This Exp.	-0.347 ± 0.008	0.	1.18
Ref. [21]	-1.55 ± 0.51	4.07 ± 1.56	0.87
Ref. [21]	-0.35 ± 0.03	0.	1.05

Systematic Errors

The systematic errors quoted throughout this analysis note were determined from the changes in the calculated results do to cut variations. Cut variations include changing the $\cos\theta_\pi$ cut from 0.75 to 0.8, removing the pxy_π cut, changing the $\cos\theta_\mu$ cut from 0.6 to 0.65, and removing the $3.07 < m_{recoil} < 3.12$ GeV/c^2 cut. In addition, the events were fitted kinematically, and a χ^2 cut was made on the fitted events. Removing the m_{recoil} cut and cutting on the kinematic fit χ^2 determines the contribution to the systematic errors due to backgrounds remaining in the event sample.

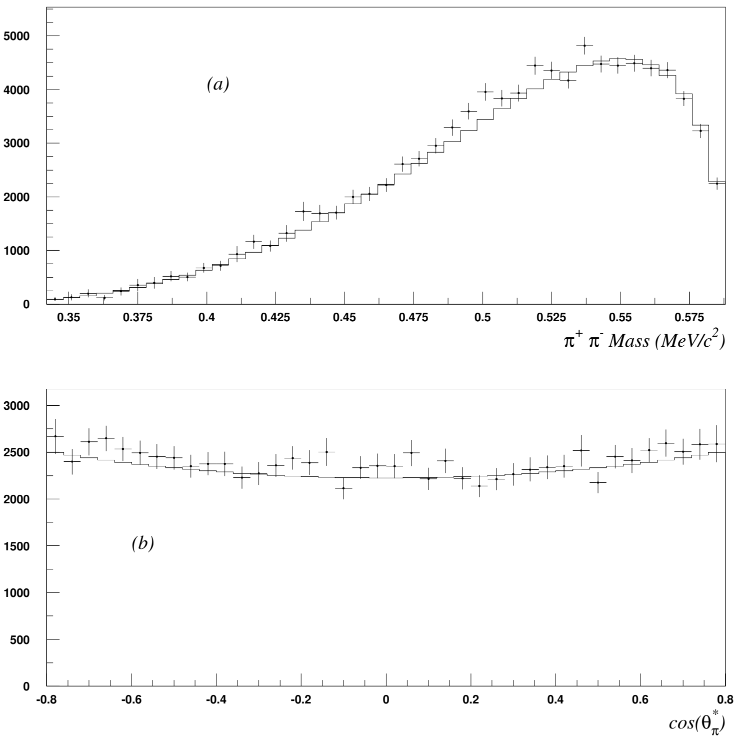

Figure 11: Fit of the 2D $\cos\theta^*_\pi$ versus $m_{\pi\pi}$ distribution to Eqn 16. **(a)** The 2D distribution projected in $m_{\pi\pi}$. **(b)** The 2D distribution projected in $\cos\theta^*_\pi$. The points are the data corrected for efficiency, and the curve is the projected fit result.

Summary

In this paper, we have studied the process $\psi' \to \pi^+\pi^- J/\psi$. We find reasonable agreement with a simple Monte Carlo model except for the distribution of $\cos\theta^*_\pi$, which is the cosine of the angle of the pion with respect to the J/ψ direction in the rest frame of the $\pi\pi$ system. This is an indication of some D-wave which was not included in the Monte Carlo.

The angular distributions are compared with the general decay amplitude analysis of Cahn. We find that $|M_{201}|/|M_{001}|$, which measures the amount of D-wave of the $\pi\pi$ system relative to the amount of S-wave, varies between 0.12 and 0.18 and is at least two sigma from zero. On the other hand $|M_{021}|/|M_{001}|$, which measures the amount of D-wave of the J/ψ - X system relative to the S-wave, varies between 0 and 0.06 and is, in all cases, consistent with zero. When we try to fit for δ^0_0, the fits have problems in Minuit. We are unable to determine the phase angle.

The $\cos\theta^*_\pi$ distribution has been fit with a simple model to determine the amount of D-wave and the amount of S-D interference as a function of $m_{\pi\pi}$. The D-wave component is very small; the S-D interference is measurable and is found to decrease with increasing $m_{\pi\pi}$ in agreement with the Novikov-Shifman model.

The $m_{\pi\pi}$ distribution has been fit with the Novikov-Shifman, T. M. Yan, T. M. Yan with higher order terms, and Voloshin-Zakorov models. The models give very similar fits except for the T. M. Yan model without higher order terms, which gives a poorer fit to the data.

In addition, the Novikov-Shifman model, which is written in terms of the parameter κ, predicts that D-wave should be present if κ is non zero. Determinations of κ based on the $\cos\theta^*_\pi$ distribution and the joint $m_{\pi\pi}$ - $\cos\theta^*_\pi$ distribution agree with the value obtained from the $m_{\pi\pi}$ distribution. The results agree well with the measurement of Argus using Mark II data.

Finally, we have fit our $m_{\pi\pi}$ $\cos\theta^*_\pi$ distribution using the Mannel-Yan model, which also allows D-wave.

References

[1] G. S. Abrams *et al.* , Phys. Rev. Lett. 34, 1181 (1975).

[2] M Voloshin, V Zakharov, Phys. Rev. Lett. 45, 688(1980).

[3] V. A. Novikov and M.A. Shifman, Z. Phys.8,43(1981).

[4] M. Shifman, Phys. Rep. 209, 341 (1991).

[5] T. M. Yan, Phys. Rev. D22, 1652 (1980). The higher order terms are given in D. Besson *et al.* , Phys. Rev. D30, 1433 (1984):

$$\begin{aligned} O(\frac{B^2)}{A^2} &= \frac{1}{20}\frac{B^2}{A^2}[(m_{\pi\pi}^2 - 4m_\pi^2)^2 + \frac{4}{3}(m_{\pi\pi}^2 - 4m_\pi^2)(m_{\pi\pi}^2 + 6m_\pi^2)\frac{K^2}{m_{\pi\pi}^2} \\ &+ \frac{8}{3}(m_{\pi\pi}^4 + 2m_\pi^2 m_{\pi\pi}^2 + 6m_\pi^4)\frac{K^4}{m_{\pi\pi}^4}] \end{aligned} \tag{18}$$

[6] Yu-Ping Kuang, T. M. Yan, Phys. Rev. D37, 1210 (1988).

[7] F. Butler *et al.* , Phys. Rev. D49, 40 (1994).

[8] F. A. Harris and Wang Meng, "Analysis Note: Number of ψ' Events", April 1998.

[9] F. A. Harris and Wang Meng, "Analysis Note: $\psi' \to \pi^+\pi^- J/\psi$, $J/\psi \to l^+l^-$ and $B(\psi' \to \pi^+\pi^- J/\psi)$", April 1998.

[10] J. Z. Bai *et al.* , "Determination of J/ψ Leptonic Branching Fraction via $\psi(2S) \to \pi^+\pi^- J/\psi$", accepted by Phys. Rev. D.

[11] BES Collaboration, "Determination of the J/ψ Leptonic Branching Fraction via $\psi(2S) \to \pi^+\pi^- J/\psi$", draft of Oct. 94.

[12] How the bin-by-bin efficiency is used depends on the type of fit being done. When the bin statistics is high, as in the 1D histograms, the data histogram is divided by the efficiency histogram, and the efficiency corrected histogram is compared to theory. When the bin statistics is small, as in the 2D histograms, and Poisson statistics becomes

important, the theory distribution is multiplied by the efficiency histogram, and the resulting histogram is compared with the detected events.

[13] The $m_{\pi\pi}$ mass resolution in this region, determined using Monte Carlo events, is 6.4 MeV/c. It should be noted that the bin-by-bin efficiency correction method compensates for the effects of resolution smearing.

[14] Robert N. Cahn, PRD 12, 3559 (1975). In the Appendix of this paper, Cahn gives the full expression for $\frac{d\Gamma}{d\Omega_\pi d\Omega_\mu d\Omega_\psi}$ in terms of all the angles involved.

[15] Belanger, et.al, PRD 39, 257 (1989); T. Ishida *et al.* , hep-ph/9712230 (Dec. 1997).

[16] We assume that δ_0^0 changes linearly as a function of $m_{\pi\pi}$.

[17] To show the relation of p and q to the S and D wave amplitudes, we can write:

$$\begin{aligned} N(\cos\theta) &\propto S^2 + \sqrt{5}SD(\cos^2\theta - 1/3) + \frac{5}{4}D^2(\cos^2\theta - 1/3)^2 \qquad (19) \\ N(\cos\theta) &\propto 1 + \sqrt{5}\frac{D}{S}(\cos^2\theta - 1/3) + \frac{5D^2}{4S^2}(\cos^2\theta - 1/3)^2 \end{aligned}$$

In the above, S and D have been treated as real. Treating them as complex numbers would add a cosine of a phase angle multiplying S/D in the interference term.

[18] Fan Jingyun *et al.* , "An Experimental Study of $\psi' \to J/\psi\pi^+\pi^-$, April 1995.

[19] H. Albrecht *et al.* , Z Phys. C 35, 283 (1987). For the $\psi(2S)$ result, Mark II data was used.

[20] J. Alexander et al., Phys. Rev. D58, 052004 (1998).D

[21] T. Mannel, Z Phys. C 73, 541 (1997).

[22] Mu-Lin Yan et al., hep-ph/9805354 (may 1998).